Article

Coumarin-Based Dual Chemosensor for Colorimetric and Fluorescent Detection of Cu²⁺ in Water Media

Nguyen Khoa Hien,[§] Mai Van Bay,[§] Nguyen Chi Bao, Quan V. Vo, Nguyen Duc Cuong, Tran Vinh Thien, Nguyen Thi Ai Nhung, Dang Ung Van, Pham Cam Nam,* and Duong Tuan Quang*

Read Online

ACCESS | Metrics & More | Article Recommendations | Supporting Information

Orange, Fluorescence ON / Pink, Fluorescence OFF
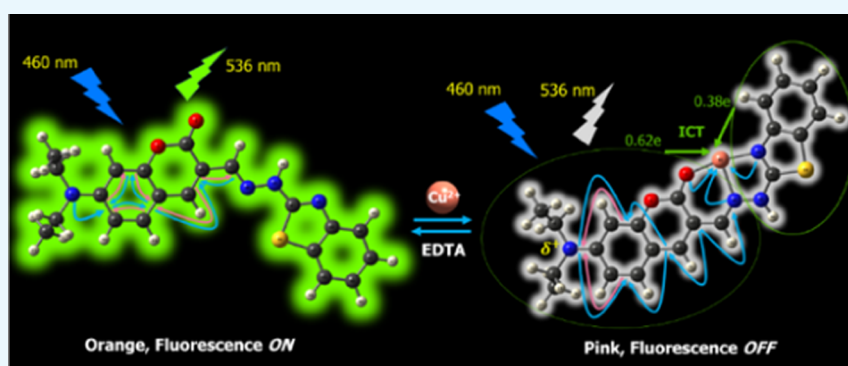
ABSTRACT: A novel coumarin derivative (**5**) was synthesized and used as a colorimetric and fluorescent probe for selective detection of Cu²⁺ ions in the presence of other metal ions, with the detection limits of 5.7 and 4.0 ppb, respectively. Cu²⁺ ion reacts with probe **5** to form a 1:1 stoichiometry complex, resulting in a remarkable redshift of absorption maximum from 460 to 510 nm, as well as almost completely quenching fluorescence intensity of probe **5** at the wavelength of 536 nm. These changes can be distinctly observed by naked eyes. In addition, the working pH range of probe **5** is wide and suitable for physiological conditions, thus probe **5** may be used for detection of Cu²⁺ ions in living cells. The stable structures of probe **5** and its 1:1 complex with Cu²⁺ ion were optimized at the PBE0/6-31+G(d) level of theory. The presence and characteristics of bonds in compounds were studied through atoms in a molecule and natural bond orbital analysis. The formation of the complex led to a strong transfer of electron density from probe **5** as a ligand to Cu²⁺ ion, resulting in breaking the π-electron conjugated system, which is the cause of fluorescence quenching and color change of **5**-Cu²⁺ complex.

1. INTRODUCTION

Copper is both an essential trace element and a toxic substance to plants, animals, and humans.[1,2] Copper toxicosis is very rare compared to its deficiency in plants.[3] This element exhibits high toxicity to microorganisms such as algae, bacteria, viruses, and aquatic animals.[4] Copper is present in almost all tissues of the human body and plays an important role in physiological processes, immunity, and resistance to oxidative stress.[5−7] The copper deficiency or copper overload is believed to be related to diseases like Alzheimer's, Parkinsons, Menkes, Wilsons, and Prion.[8−11]

There are different methods that can determine Cu²⁺ ions at ppb levels such as absorption atomic spectrometry (AAS),[12,13] inductively coupled plasma mass spectrometry (ICP-MS),[14] inductively coupled plasma optical emission spectrometry (ICP-OES),[15] and voltammetry.[16] However, these methods require expensive equipment, with complicated sample preparation and measurement techniques. Meanwhile, a fluorescence-based analytical method can also determine

Cu²⁺ ions at ppb levels, which is simpler and less expensive than the above methods.[17,18] Furthermore, a fluorescence-based analytical method can be used to monitor substances in living cells to detect abnormal cases and causes of diseases.[19−21] Therefore, the development of new fluorescent probes for Cu²⁺ ions has attracted special attention of scientists.[22−24] So far, many fluorescent probes for Cu²⁺ ions have been reported. The development of new fluorescent probes is, however, still being concerned due to the limitations of reported probes such as low sensitivity and selectivity,[25,26] a narrow range of pH,[20,27−29] working in solutions with a high proportion of organic solvents,[26,30] and excitation wavelength
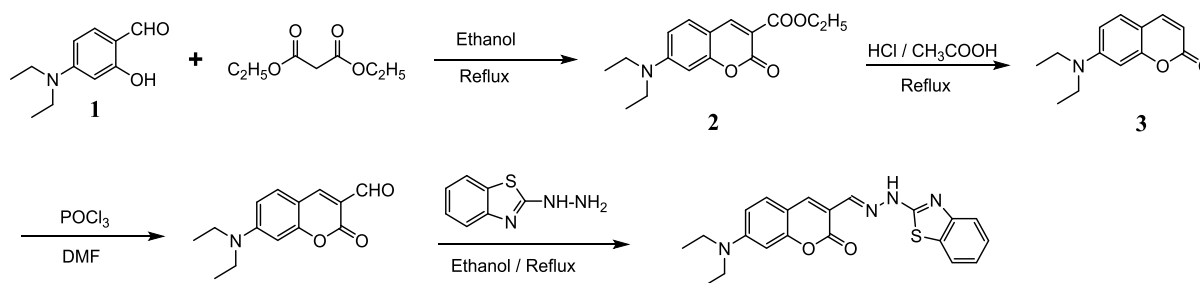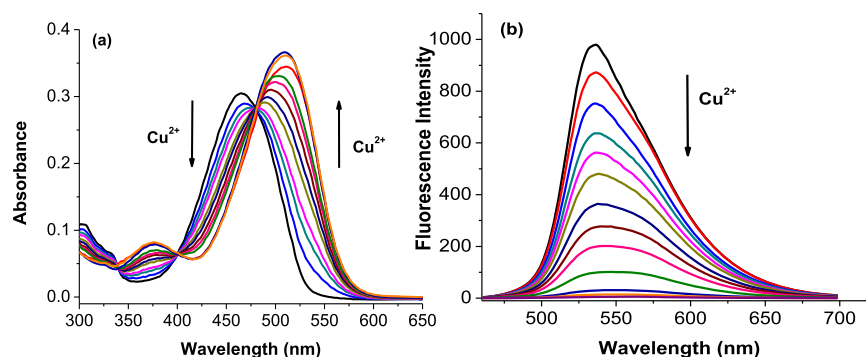
Figure 1. Synthetic pathway for the probe **5**.

Figure 2. (a) Absorbance titration spectra of probe **5** (5 μM) in ethanol/4-(2-hydroxyethyl)-1-piperazineethanesulfonic acid (HEPES, pH 7.4, 1/1, v/v) at 25 °C with gradual addition of 0, 0.1, 0.2, 0.3, 0.4, 0.5, 0.6, 0.7, 0.8, 0.9, 1.0, 1.5, and 2.0 equiv of Cu^{2+} ions. (b) Fluorescence titration spectra of probe **5** (5 μM) in ethanol/HEPES (pH 7.4, 1/1, v/v) at 25 °C with gradual addition of 0, 0.1, 0.2, 0.3, 0.4, 0.5, 0.6, 0.7, 0.8, 0.9, 1.0, 1.5, and 2.0 equiv of Cu^{2+} ions with an excitation of 460 nm.
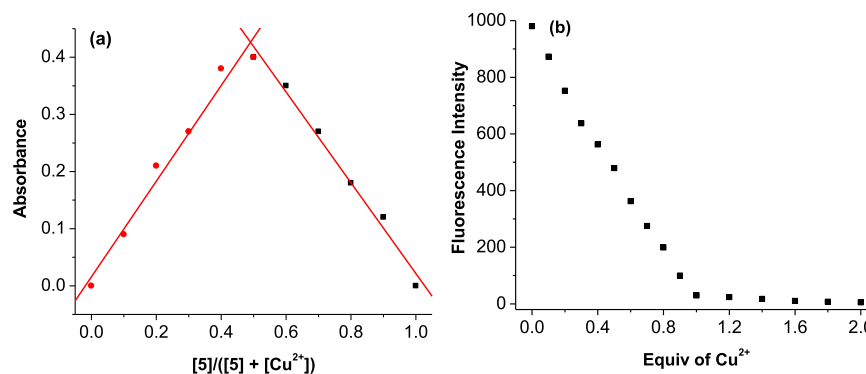

Figure 3. (a) Job plot of probe **5** and Cu^{2+} ions. (b) Plot and linear fitting of the fluorescence intensity of probe **5** (5 μM) with different concentrations of Cu^{2+} ions (excitation wavelength: 460 nm, emission wavelength: 536 nm).

in the ultraviolet region.[26,28,31,32] These limitations reduce the application of probes to monitor Cu^{2+} ions in living cells.

In this study, a novel derivative of coumarin, (E)-3-((2-(benzo[d]thiazol-2-yl)hydrazono)methyl)-7-(diethylamino)-coumarin (**5**) that was successfully synthesized could be used as a colorimetric and fluorescent probe for detection of Cu^{2+} ions in the preeminent operating conditions such as high sensitivity and selectivity, a wide range of pH, and excitation wavelength in the visible region. In addition, quantum chemical calculations have also been used to determine the optimized geometry of **5**-Cu^{2+} complex and shed light on the cause of the changes in fluorescence properties.

2. RESULTS AND DISCUSSION

2.1. Synthesis of (E)-3-((2-(Benzo[d]thiazol-2-yl)-hydrazono)methyl)-7-(diethylamino)coumarin (5). Probe **5** was synthesized through four steps as shown in

Figure 1. First, 7-diethylamino-3-ethylacetate-coumarin (**2**) was synthesized from a condensation reaction between 4-diethylaminosalicylaldehyde (**1**) and diethylmalonate in the presence of triethylamine. Second, 7-diethylamino-coumarin (**3**) was obtained from the decarboxylation reaction of **2** using concentrated HCl and glacial acetic acid. Third, 7-diethylami-nocoumarin-3-aldehyde (**4**) was obtained from the aldehyde reaction of **3** in the presence of POCl$_3$ and N,N-dimethylformamide (DMF). Finally, probe **5** was obtained from the condensation reaction of 7-diethylaminocoumarin-3-aldehyde (**4**) with 2-hydrazinobenzothiazole in about 30% overall yield (Supporting Information). The structures of the products **3**, **4**, **5**, and intermediates were confirmed by ^{1}H NMR, ^{13}C NMR, and electrospray ionization mass spectrom-etry (ESI-MS) analysis (Figures S1−S4, Supporting Informa-tion).
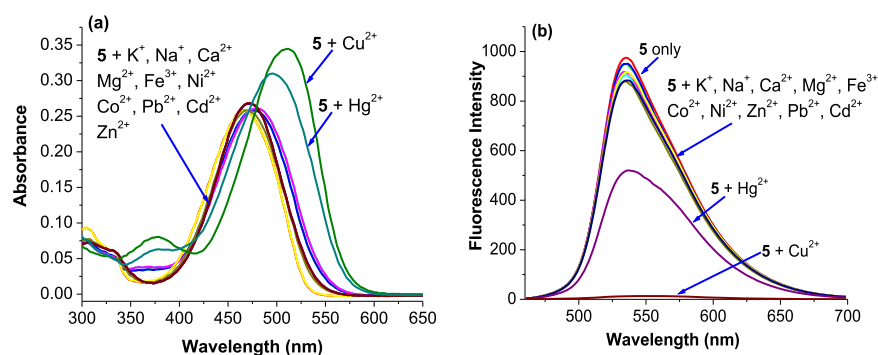
Figure 4. Absorption spectra (a) and fluorescence spectra (b) of probe **5** (5 μM) in ethanol/HEPES (pH 7.4, 1/1, v/v) at 25 °C upon addition of 1 equiv of Cu^{2+} ions and other metal ions including Na^+, K^+, Ca^{2+}, Mg^{2+}, Fe^{3+}, Co^{2+}, Ni^{2+}, Zn^{2+}, Pb^{2+}, Cd^{2+}, and Hg^{2+} ions (excitation wavelength: 460 nm, emission wavelength: 536 nm).
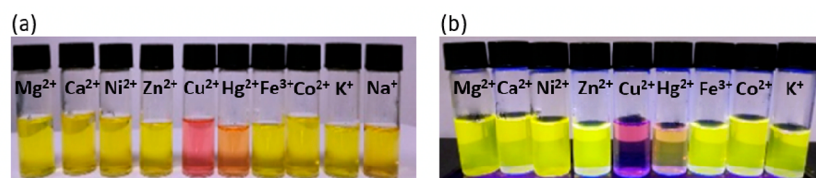
Figure 5. Color changes (a) and fluorescence changes (b) of probe **5** with Na^+, K^+, Ca^{2+}, Mg^{2+}, Fe^{3+}, Co^{2+}, Ni^{2+}, Cu^{2+}, Zn^{2+}, Pb^{2+}, Cd^{2+}, Cu^{2+}, and Hg^{2+}.
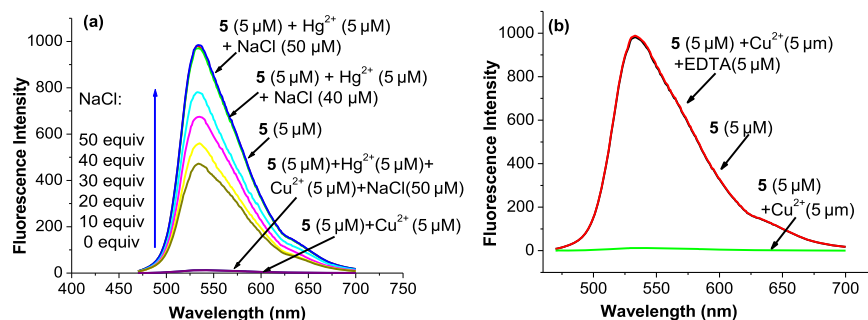
Figure 6. Fluorescence spectra of probe **5** (5 μM) in ethanol/HEPES (pH 7.4, 1/1, v/v) at 25 °C (a) upon addition of 1 equiv of Hg^{2+} ions and NaCl (0−50 μM) and (b) upon addition of 1 equiv of Cu^{2+} ions and EDTA (50 μM) (excitation wavelength: 460 nm).

## 2.2. Experimental Characterization and Application of Probe 5.

The absorption and fluorescence titration spectra of probe **5** with Cu^{2+} ions in aqueous solution are presented in Figure 2. It shows that free probe **5** has a characteristic absorption band peaked at the wavelength of 460 nm in aqueous solution. The absorption maximum is progressively redshifted with gradual addition of Cu^{2+} ions. The absorption maximum at 460 nm is gradually decreased, whereas a new absorption maximum at 510 nm appears. In companion with this, there is a change in the color of the solution from orange to pink. Furthermore, three distinct isosbestic points are observed at 340, 400, and 475 nm. These results indicate that the concentration of the light-absorbing compounds has been converted back and forth in the solution. This is seen as a piece of evidence for the formation of a new compound between probe **5** and Cu^{2+} ions.[33−35]

As shown in Figure 2, free probe **5** has a strong emission band peaked at the wavelength of 536 nm with an excitation wavelength of 460 nm. The fluorescence quantum yield (Φ) of free probe **5** in aqueous solution is determined to be 10.5%, using the fluorescein in 0.1 N NaOH solution as a reference.[36] Addition of Cu^{2+} ions greatly quenches the fluorescence

intensity of probe **5**, along with a slight redshift in the emission maximum. Upon addition of 1 equiv of Cu^{2+} ions to the solution of probe **5**, the fluorescence intensity is quenched over 95% of its original intensity, along with a shift in the emission maximum from 536 to 545 nm. The fluorescence quantum yield (Φ) of the product between probe **5** and Cu^{2+} ions in aqueous solution is found to be 0.15% based on the obtained experimental data.

The Job plot in Figure 3a shows a complexation between probe **5** and Cu^{2+} ions in a molar ratio of 1:1. The stoichiometry is also confirmed by the plot of the fluorescence intensity of probe **5** with different concentrations of Cu^{2+} ions. Figure 3b shows that the fluorescence intensity is gradually quenched upon an increasing addition of Cu^{2+} ions. Upon addition of 1 equiv of Cu^{2+} ions, the fluorescence intensity is quenched to more than 95% and then becomes almost unchanged as the concentration of Cu^{2+} ions is further increased.

The selectivity of probe **5** toward Cu^{2+} ions compared to the other metal ions was investigated. Figure 4 gives the variations of absorption and fluorescence spectra of probe **5** caused by miscellaneous ions including Na^+, K^+, Ca^{2+}, Mg^{2+}, Fe^{3+}, Co^{2+},
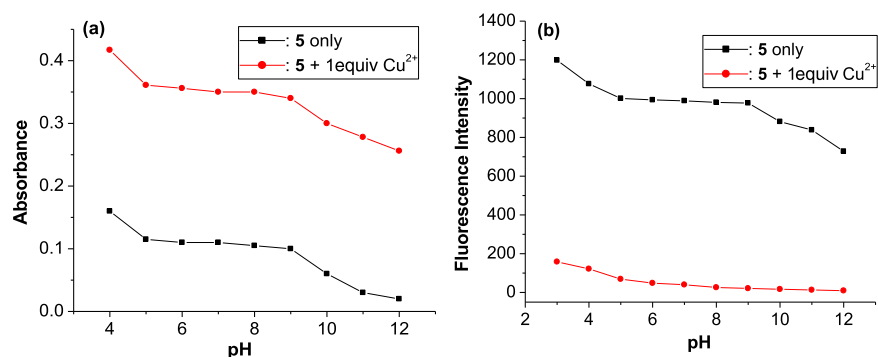
Figure 7. (a) Absorption intensity at 510 nm and (b) fluorescence intensity at 536 nm of probe **5** (5 μM) in the absence and presence of 1 equiv of Cu^{2+} ions in ethanol/HEPES (pH 7.4, 1/1, v/v) solution.
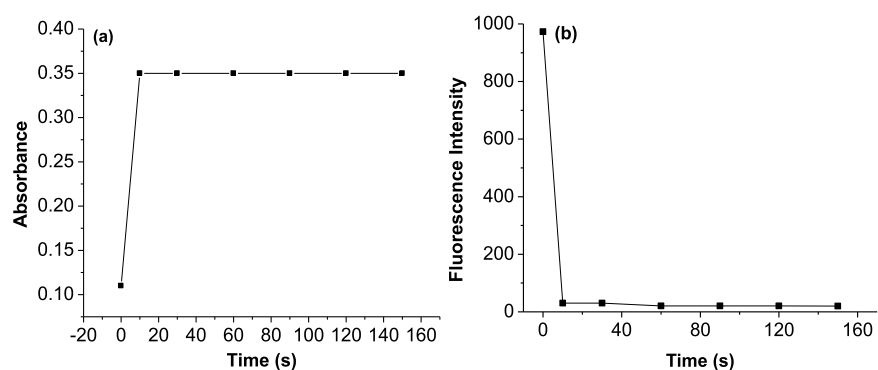
Figure 8. (a) Changes of absorbance at 510 nm and (b) fluorescence intensity at 536 nm of probe **5** (5 μM) after adding 1 equiv of Cu^{2+} ions in ethanol/HEPES (pH 7.4, 1/1, v/v) with different times.
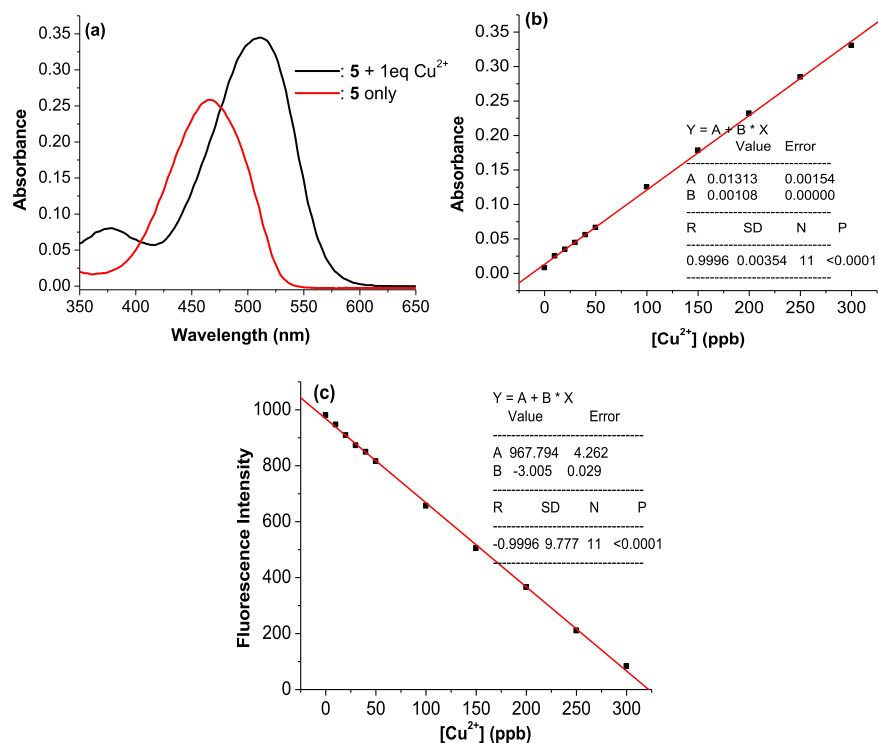
Figure 9. (a) Absorption spectra of probe **5** (5 μM) and probe **5** (5 μM) + 1 equiv of Cu^{2+} ions in ethanol/HEPES (pH 7.4, 1/1, v/v). (b) Variation of absorbance at 525 nm of **5** solution (5 μM) in ethanol/HEPES (pH 7.4, 1/1, v/v) versus the concentration of Cu^{2+} ions (0–300 ppb). (c) Variation of fluorescence intensity at 536 nm of **5** solution (5 μM) in ethanol/HEPES (pH 7.4, 1/1, v/v) versus the concentration of Cu^{2+} ions (0–300 ppb).

Ni^{2+}, Zn^{2+}, Pb^{2+}, Cd^{2+}, Hg^{2+}, and Cu^{2+} ions. The results show that Cu^{2+} ions cause a remarkable redshift in absorption maximum from 460 to 510 nm with increased intensity; Hg^{2+} ions induce a medium change from 460 to 500 nm, whereas other metal ions only produce slight changes in their absorption spectra (Figure 4a). On the other hand, probe **5** shows a strong emissive band peaked at 536 nm. Cu^{2+} ions can quench the fluorescence of probe **5** to more than 95%, whereas Hg^{2+} ions can quench fluorescence to about 40%. Other miscellaneous competitive ions do not lead to any significant changes in fluorescence (Figure 4b). The above changes in color and fluorescence can be distinctly observed by naked eyes, and their photos are presented in Figure 5. All these show a remarkably high selectivity of probe **5** for Cu^{2+} ions over other competitive ions except for Hg^{2+} ions.

The possibility of using probe **5** to quantify Cu^{2+} ions in the presence of Hg^{2+} ions is also investigated. As shown in Figure 6a, the influence of Hg^{2+} ions on the quantification of Cu^{2+} ions can be prevented by adding 8−10 equiv of NaCl to the solution containing Hg^{2+} ions. Furthermore, when 10 equiv of Na$_4$ EDTA is added to the solution of probe **5** containing 1 equiv of Cu^{2+} ions, the solution returns to strong fluorescence with the same intensity as the solution of free probe **5** (Figure 6b). This result shows that the reaction between Cu^{2+} ions and probe **5** is reversible. Therefore, probe **5** acts as a chemosensor for Cu^{2+} ions.

For practical applicability, a proper range of pH values for probe **5** was also evaluated. Figure 7a shows that the absorbance of free probe **5** and of probe **5** in the presence of Cu^{2+} ions reaches a plateau in the pH range from 5 and 9. Under acidic conditions (pH < 5) or alkaline conditions (pH > 9), the absorbance of these solutions is not stable upon pH changes, it decreases as pH increases. A similar result also comes from the fluorescence spectra with the change of pH conditions, as presented in Figure 7b. These results show that probe **5** can detect Cu^{2+} ions with a wide pH span, from 5 to 9.

The changes of absorbance and fluorescence intensity of probe **5** (5 μM, in ethanol/HEPES, pH 7.4, 1/1, v/v) after adding 1 equiv of Cu^{2+} ions with different times are investigated and presented in Figure 8. The results show that the complexation process between probe **5** with Cu^{2+} ions is very fast. It can reach the equilibrium within several seconds, indicating that probe **5** can be used for real-time detection of Cu^{2+} ions.

The possibility to use **5** as a chemosensor for quantification of Cu^{2+} ions by colorimetric and fluorescent methods was investigated. The results obtained from the absorption spectra show that the optimal absorption wavelength for quantification of Cu^{2+} ions is 525 nm, where the difference between absorbances is the largest, and the absorbance of Cu^{2+} ions is approximately equal to zero (Figure 9a). Figure 9b,c show that, in the concentration range of Cu^{2+} ions from 0 to 300 ppb, the linear relationships between the concentration of Cu^{2+} ions and the absorbance or fluorescence intensity of **5** solution (5 μM) are very good and expressed by the equations that were found from calibration curves: $A_{525 nm} = (0.013 \pm 0.002) + (0.001 \pm 0.000) \times [Cu^{2+}]$ (ppb) or $FI_{536 nm} = (967.793 \pm 4.262) - (3.004 \pm 0.029) \times [Cu^{2+}]$ (ppb). The calculated linear correlation coefficients are 0.9996 and 0.9996, respectively. These results indicate that **5** can be used as a colorimetric or fluorescent chemosensor for quantification of Cu^{2+} ions. The limit of detection is 5.7 ppb for the colorimetric method and 4.0 ppb for the fluorescent method (Figure S5),

much lower than that for the recently published colorimetric and fluorescent sensors.[37−40] The method of using probe **5** to quantify Cu^{2+} ions in the presence or absence of Hg^{2+} ions has been assessed for accuracy through the repeatability (relative standard deviation, RSD) and recovery rate. The obtained results were reliable (see more details in Supporting Information).

2.3. Investigations on the Structural Properties of Probe 5 and Its Complex with Cu^{2+} ions. For the optimized geometries of probe **5**, the 1:1 complexes between probe **5** and Cu^{2+} ions were optimized at the PBE0/6-31+G(d) level of theory. The stable structures corresponding to minima on the potential energy surface are shown in Figure 10. All their Cartesian coordinates are presented in Tables S1
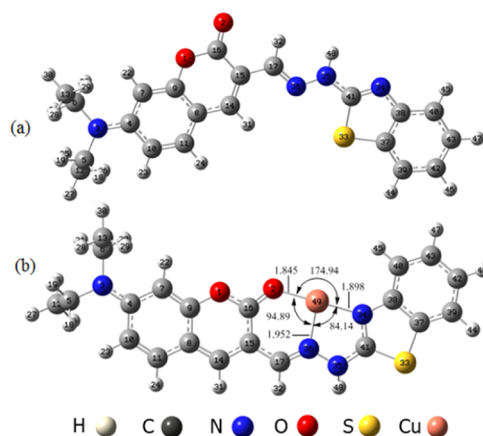
Figure 10. Stable structures of probe **5** (a) and its 1:1 complex with Cu^{2+} ions (b) at the PBE0/6-31+G(d) level of theory.

and S2 of Supporting Information. The calculated bond lengths, bond angles, and dihedral angles of probe **5** and its 1:1 complex with Cu^{2+} ions are presented in Table S3 of Supporting Information.
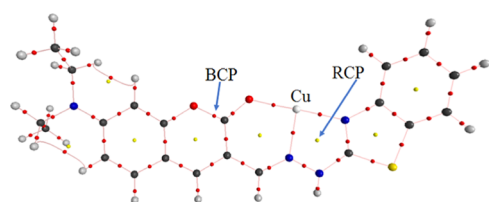
The calculated results show that in free probe **5**, most of the atoms are coplanar except for the ones of ethylamino groups. Two chains C(16)−C(15)−C(17)−N(36) and N(36)−N(35)−C(41)−N(34) in free probe **5** are in *trans*-configurations (Figure 10a). Meanwhile, the 1:1 complexation leads to the changes in configurations of these two chains, being cis-configuration (Figure 10b).

The calculated values of $\rho(r)$ and $\nabla^2(\rho(r))$ and the topological properties of **5**-Cu^{2+} complex at the critical points obtained from AIM analysis are presented in Table 1 and Figure 11, respectively. The calculated results confirmed the presence of chemical bonds in each of the O(2)···Cu(49), N(36)···Cu(49), and N(34)···Cu(49) contacts. All values of $\nabla^2(\rho(r))$ for these contacts are negative. In addition, the contact distances of atom pairs O(2)···Cu(49), N(36)···Cu(49), and N(34)···Cu(49) are 1.845, 1.952, and 1.898 Å, respectively. They are significantly smaller than the sum of the van der Waals atomic radii of corresponding atom pairs (2.920, 2.950, and 2.950 Å). As a result, these contacts are thought to form covalent bonds. RCPs are found in the center of O(2)···C(16)···C(15)···C(17)···N(36)···Cu(49) and N(36)···N(35)···C(41)···N(34)···Cu(49) atom groups, indicating a cyclic structure present in each group of atoms.

The intermolecular orbital interaction and bond properties are investigated by natural bond orbital (NBO) analysis to

Table 1. Electron density ($\rho(r)$, in au) and the Laplacian ($\nabla^2(\rho(r))$, in au) at the contact points of atom pairs in 5-Cu^{2+} complex at the PBE0/6-31+G(d) level of theory

bond	$\rho(r)$	λ_1	λ_2	λ_3	$\nabla^2(\rho(r))$	critical point
O(2)···Cu(49)	0.1127	−0.1589	−0.1573	0.9036	−0.1469	BCP
N(36)···Cu(49)	0.1032	−0.1393	−0.1343	0.6041	−0.0826	BCP
N(34)···Cu(49)	0.1148	−0.1525	−0.1488	0.6977	−0.0991	BCP
O(2)···C(16)···C(15)···C(17)···N(36)···Cu(49)	0.0146	−0.0101	0.0367	0.0526	−0.0198	RCP
N(36)···N(35)···C(41)···N(34)···Cu(49)	0.0275	−0.0229	0.0642	0.1283	−0.0424	RCP

Figure 11. Topological properties of 5-Cu^{2+} complex at the BCPs (yellow points) and RCPs (red points).

explain the fluorescent properties of probe **5** and 5-Cu^{2+} complex. The calculated results in Table 2 and Figure 11 show that in free probe **5**, the presence of π bonds between atom pairs with their significantly large interactive energies ($E^{(2)}$), including C4−C10, C11−C8, C14−C15, C17−C36, and O2−C16, has led to the formation of a π-electron conjugated system in the first moiety of probe **5** containing the diethylaminocoumarin. This π-electron conjugated system also enhances electron density from the electron pair of the N3 atom by the donor−acceptor interaction, with the interactive

Table 2. Significant second-order interaction energies at the PBE0/6-31+G(d) level of theory (kcal·mol^{-1}) between donor and acceptor orbitals in 5 and 5-Cu^{2+} complex

donor NBO (i)	acceptor NBO (j)	$E^{(2)}$	donor NBO (i)	acceptor NBO (j)	$E^{(2)}$
5			**5-Cu^{2+}**		
π(C4−C10)	π*(C7−C9)	14.80	π(C7−C9)	π*(N3−C4)	14.05
π(C4−C10)	π*(C8−C11)	32.07	π(C8−C14)	π*(C7−C9)	12.19
π(C7−C9)	π*(C4−C10)	24.47	π(C10−C11)	π*(N3−C4)	13.15
π(C7−C9)	π*(C8−C11)	13.91	π*(N3−C4)	π*(C7−C9)	48.82
π(C8−C11)	π*(C4−C10)	17.70	π*(N3−C4)	π*(C10−C11)	24.57
π(C8−C11)	π*(C7−C9)	27.97	π*(C8−C14)	π*(C10−C11)	23.42
π(C8−C11)	π*(C14−C15)	24.83	LP(O1)	LP*(C16)	43.31
π(C14−C15)	π*(O2−C16)	27.96	LP(O1)	π*(C7−C9)	14.11
π(C14−C15)	π*(C8−C11)	13.99	LP(O2)	LP*(C16)	64.86
π(C14−C15)	π*(C17−N36)	19.81	LP(C15)	π*(C8−C14)	30.79
LP (O1)	π*(O2−C16)	40.59	LP(C15)	π*(C17−N36)	57.01
LP (O1)	π*(C7−C9)	33.17	LP(N35)	π*(C17−N36)	12.97
LP (O2)	δ*(O1−C16)	39.11	LP(O2)	LP*(Cu49)	13.89
LP (O2)	δ*(C15−C16)	18.09	LP(O2)	LP*(Cu49)	20.19
LP (N3)	π*(C4−C10)	52.50	LP(N34)	LP*(Cu49)	19.52
δ*(O1−C16)	δ*(O1−C9)	22.77	LP(N34)	LP*(Cu49)	23.49
π*(O2−C16)	π*(C14−C15)	125.95	LP(N34)	LP*(Cu49)	11.14
π*(C4−C10)	π*(C8−C11)	431.68	LP(N36)	LP*(Cu49)	14.70
π*(C8−C11)	π*(C14−C15)	218.22	LP(N36)	LP*(Cu49)	29.53
π*(C17−N36)	π*(C14−C15)	76.60	π(C37−C39)	LP*(C42)	20.29
π*(C4−C10)	π*(C7−C9)	352.98	π(C37−C39)	π*(N34−C38)	13.32
π(N34−C41)	π*(C37−C38)	18.64	π(C40−C43)	LP*(C42)	22.65
π(C37−C38)	π*(N34−C41)	10.85	π(C40−C43)	π*(N34−C38)	19.41
π(C37−C38)	π*(C39−C42)	21.99	π*(N34−C38)	π*(C37−C39)	42.65
π(C37−C38)	π*(C40−C43)	17.54	π*(N34−C38)	π*(C40−C43)	29.85
π(C39−C42)	π*(C37−C38)	19.24	LP(C41)	π*(N34−C38)	24.08
π(C39−C42)	π*(C40−C43)	20.75	LP*(C42)	π*(C37−C39)	51.77
π(C40−C43)	π*(C37−C38)	22.80	LP*(C42)	π*(C40−C43)	34.21
π(C40−C43)	π*(C39−C42)	20.58	π(C34−C38)	LP*(C41)	45.19
LP (S33)	π*(N34−C41)	29.69	LP(N35)	π*(C17−N36)	12.97
LP (S33)	π*(C37−C38)	17.92	LP(S33)	LP(C41)	66.00
LP (N34)	δ*(S33−C41)	19.21	LP(N35)	LP(C41)	47.19
LP (N35)	π*(C17−N36)	33.15			
LP (N35)	π*(N34−C41)	53.86			
π*(N34−C41)	π*(C37−C38)	119.73			
π*(C37−C38)	π*(C39−C42)	197.32			
π*(C37−C38)	π*(C40−C43)	158.69			

energy ($E^{(2)}$) of 52.50 kcal·mol^{-1}. These intermolecular orbital interaction and bond properties are typical in fluorescent compounds.[41−43] These findings are considered as evidence for the fluorescence of probe **5**.

In **5**-Cu^{2+} complex, the binding between **5** ligand and Cu^{2+} ion is stabilized by the electron donor−acceptor interactions between electron lone pairs (LP) on the O and N atoms of the ligand and on the Cu atom. The hyperconjugation energies of the LP(2)O2 → LP*(5)Cu49, LP(2)O2 → LP*(6)Cu49, LP(1)N34 → LP*(5)Cu49, LP(1)N34 → LP*(6)Cu49, LP(1)N34 → LP*(7)Cu49, LP(1)N36 → LP*(5)Cu49, and LP(1)N36 → LP*(6)Cu49 in the complex are 13.89, 20.19, 19.52, 23.49, 11.14, 14.70, and 29.53 kcal·mol^{-1}, respectively. These interactions have caused a strong transfer of electron density from **5** ligand to Cu^{2+} ion. The calculated charge of Cu atom in **5**-Cu^{2+} complex is +1.00e, indicating that **5** ligand becomes deficient in electron density. The charge of the first moiety of **5** in the complex is +0.62e, while the charge of the second moiety of **5** in the complex is +0.38e. The charge values of C17 and N3 in the complex are significantly more positive than those in free **5** (The NBO charges of atoms are presented in Table S4). The deficiency in electron density at C17 and N3 has resulted in breaking the π-electron conjugated system in the first moiety of **5** at the C15 atom. The π bonds between C15−C14 or C15−C17 are not found, while the LP(1)C15 → π^*(C8−C14) and LP(1)C15 → π^*(C17−N36) interactions are found with the hyperconjugation energies of 30.79 and 57.01 kcal·mol^{-1}, respectively. On the other hand, the calculated results have confirmed the presence of the π(N3−C4) bond and the absence of interactions from the electron lone pairs of the N3 atom in the form of donor−acceptor interaction. These findings shed light on the cause of fluorescence quenching in **5**-Cu^{2+} complex.

3. CONCLUSIONS

A novel coumarin derivative was synthesized and could be used as a colorimetric and fluorescent probe for detection of Cu^{2+} ions with the detection limits of 5.7 and 4.0 ppb, respectively. This probe could operate over a wide range of pH from 5 to 9 and was not affected by the presence of other metal ions, including Na$^+$, K$^+$, Ca^{2+}, Mg^{2+}, Fe^{3+}, Co^{2+}, Ni^{2+}, Zn^{2+}, Pb^{2+}, Cd^{2+}, and Hg^{2+}. The stable structures of probe **5** and its 1:1 complex with Cu^{2+} ions have been identified at the PBE0/6-31+G(d) level of theory and is confirmed by AIM analysis. The results from NBO analysis showed that the formation of the complex led to a strong transfer of electron density from **5** ligand to Cu^{2+} ion. As a result, the π-electron conjugated system was broken, resulting in fluorescence quenching and color change in the complex.

4. MATERIALS AND METHODS

4.1. Instruments. A Shimadzu UV-1800 UV−Vis spectrophotometer was used for the UV−Vis absorption spectra. A Shimadzu RF-5301PC series fluorescence spectrometer was used for the fluorescence spectra. A Varian instrument was used for the ^{1}H NMR and ^{13}C NMR spectra. A Finnigan 4021C instrument and Daltonics flex analysis software were used for the mass spectra.

4.2. Reagents. 4-Diethylaminosalicylaldehyde, diethylmalonate, 2-hydrazinobenzothiazole, triethylamine, acetic acid, HEPES, POCl$_3$, HCl, NaOH, and all ions of Na$^+$, K$^+$, Ca^{2+}, Mg^{2+}, Fe^{3+}, Co^{2+}, Ni^{2+}, Hg^{2+}, Zn^{2+}, Pb^{2+}, Cd^{2+}, and Cu^{2+} as

their chloride or perchlorate were purchased from Aldrich Chemical Corporation and used as received. DMF was an HPLC reagent and redistilled prior to use. Ethanol was of HPLC grade without fluorescent impurity. All solvents were purchased from Merck and used as received. Deionized water was used for all experiments.

4.3. Computational Methodology. The optimized geometries of compounds were determined at the PBE0/6-31+G(d) level of theory,[44−46] using the Gaussian 09 program package.[47,48] The structures and the nature of the bonds in these compounds have also been investigated through the atoms in molecules (AIM) topological analysis,[49] using the AIM2000 software.[50] The calculated results, including the electron density ($\rho(r)$), Laplacian $\nabla^2(\rho(r))$, the bond critical points (BCPs), and the ring critical points (RCPs), were used to evaluate the stability of bonds, the characteristics of bonds, the presence of bonds, and ring structure.[41,51−53] The electronic properties of compounds were investigated by the natural bond orbital (NBO) analysis, using the NBO 3.1 program available in Gaussian 09 package, at the PBE0/6-31+G(d) level of theory. The calculated results, including NBO charge of atoms, the second-order stabilization energy ($E^{(2)}$) between the donor NBO(i) and the acceptor NBO(j), were used to evaluate interactions and shed light on the fluorescent characteristics of compounds.[41,54−57]

■ ASSOCIATED CONTENT

ⓈI Supporting Information

The Supporting Information is available free of charge at https://pubs.acs.org/doi/10.1021/acsomega.0c03097.

■ AUTHOR INFORMATION

Corresponding Authors

Pham Cam Nam − *The University of Danang-University of Science and Technology, Danang 550000, Vietnam*; Email: pcnam@dut.udn.vn

Duong Tuan Quang − *University of Education, Hue University, Hue 530000, Vietnam*; ● orcid.org/0000-0002-4926-0271; Email: dtquang@hueuni.edu.vn

Authors

Nguyen Khoa Hien − *Mientrung Institute for Scientific Research, Vietnam Academy of Science and Technology, Hue 530000, Vietnam*

Mai Van Bay − *University of Education, Hue University, Hue 530000, Vietnam; The University of Danang-University of Science and Education, Danang 550000, Vietnam*

Nguyen Chi Bao − *Hue University, Hue 530000, Vietnam*

Quan V. Vo − *Faculty of Chemical Technology-Environment, The University of Danang-University of Technology and Education, Danang 550000, Vietnam*; ● orcid.org/0000-0001-7189-9584

Nguyen Duc Cuong − *Hue University, Hue 530000, Vietnam*

Tran Vinh Thien − *Faculty of Geology & Mineral Resources Engineering, Ho Chi Minh University of Natural Resources and Environment, Ho Chi Minh 700000, Vietnam*

Nguyen Thi Ai Nhung − *University of Sciences, Hue University, Hue 530000, Vietnam*; ● orcid.org/0000-0002-5828-7898

Dang Ung Van − *Hoa Binh University, Hanoi 100000, Vietnam*

■ REFERENCES

(1) Willis, M. S.; Monaghan, S. A.; Miller, M. L.; McKenna, R. W.; Perkins, W. D.; Levinson, B. S.; Bhushan, V.; Kroft, S. H. Zinc-induced copper deficiency: a report of three cases initially recognized on bone marrow examination. *Am. J. Clin. Pathol.* **2005**, *123*, 125−131.

(2) Robinson, N. J.; Winge, D. R. Copper metallochaperones. *Annu. Rev. Biochem.* **2010**, *79*, 537−562.

(3) Klevay, L. M. Copper as a supplement to iron for hemoglobin building in the rat (Hart et al., 1928). *J. Nutr.* **1997**.

(4) Lawrence, C.; Sanders, G. E.; Wilson, C. Aquatics. *Management of Animal Care and Use Programs in Research, Education, and Testing*, 2nd ed.; CRC Press/Taylor & Francis, 2018.

(5) Valko, M.; Jomova, K.; Rhodes, C. J.; Kuča, K.; Musílek, K. Redox- and non-redox-metal-induced formation of free radicals and their role in human disease. *Arch. Toxicol.* **2016**, *90*, 1−37.

(6) Banci, L.; Bertini, I.; Ciofi-Baffoni, S.; Kozyreva, T.; Zovo, K.; Palumaa, P. Affinity gradients drive copper to cellular destinations. *Nature* **2010**, *465*, 645−648.

(7) Matak, P.; Zumerle, S.; Mastrogiannaki, M.; El Balkhi, S.; Delga, S.; Mathieu, J. R. R.; Canonne-Hergaux, F.; Poupon, J.; Sharp, P. A.; Vaulont, S.; Peyssonnaux, C. Copper deficiency leads to anemia, duodenal hypoxia, upregulation of HIF-2α and altered expression of iron absorption genes in mice. *PLoS One* **2013**, *8*, No. e59538.

(8) Haywood, S. Brain−Barrier Regulation, Metal (Cu, Fe) Dyshomeostasis, and Neurodegenerative Disorders in Man and Animals. *Inorganics* **2019**, *7*, 108.

(9) Montes, S.; Rivera-mancia, S.; Diaz-ruiz, A.; Tristan-lopez, L.; Camilo, R. Review article copper and copper proteins in Parkinson's disease. *Oxid. Med. Cell. Longevity* **2014**, *2014*, 1−15.

(10) Yasmeen, S.; Lund, K.; De Paepe, A.; De Bie, S.; Heiberg, A.; Silva, J.; Martins, M.; Skjørringe, T.; Møller, L. B. Occipital horn syndrome and classical Menkes Syndrome caused by deep intronic mutations, leading to the activation of ATP7A pseudo-exon. *Eur. J. Hum. Genet.* **2014**, *22*, 517−521.

(11) Weiss, K. H.; Runz, H.; Noe, B.; Gotthardt, D. N.; Merle, U.; Ferenci, P.; Stremmel, W.; Füllekrug, J. Genetic analysis of BIRC4/XIAP as a putative modifier gene of Wilson disease. *J. Inherited Metab. Dis.* **2010**, *33*, 233−240.

(12) Doner, G.; Ege, A. Determination of copper, cadmium and lead in seawater and mineral water by flame atomic absorption spectrometry after coprecipitation with aluminum hydroxide. *Anal. Chim. Acta* **2005**, *547*, 14−17.

(13) Lin, T.-W.; Huang, S.-D. Direct and simultaneous determination of copper, chromium, aluminum, and manganese in urine with a multielement graphite furnace atomic absorption spectrometer. *Anal. Chem.* **2001**, *73*, 4319−4325.

(14) Becker, J. S.; Matusch, A.; Depboylu, C.; Dobrowolska, J.; Zoriy, M. Quantitative imaging of selenium, copper, and zinc in thin sections of biological tissues (Slugs− Genus Arion) measured by laser ablation inductively coupled plasma mass spectrometry. *Anal. Chem.* **2007**, *79*, 6074−6080.

(15) Otero-Romaní, J.; Moreda-Piñeiro, A.; Bermejo-Barrera, P.; Martin-Esteban, A. Inductively coupled plasma−optical emission spectrometry/mass spectrometry for the determination of Cu, Ni, Pb and Zn in seawater after ionic imprinted polymer based solid phase extraction. *Talanta* **2009**, *79*, 723−729.

(16) Buffle, J.; Tercier-Waeber, M.-L. Voltammetric environmental trace-metal analysis and speciation: from laboratory to in situ measurements. *TrAC, Trends Anal. Chem.* **2005**, *24*, 172−191.

(17) Aragay, G.; Pons, J.; Merkoçi, A. Recent trends in macro-, micro-, and nanomaterial-based tools and strategies for heavy-metal detection. *Chem. Rev.* **2011**, *111*, 3433−3458.

(18) Chen, Y.; Min, X.; Zhang, X.; Zhang, F.; Lu, S.; Xu, L.-P.; Lou, X.; Xia, F.; Zhang, X.; Wang, S. AIE-based superwettable microchips for evaporation and aggregation induced fluorescence enhancement biosensing. *Biosens. Bioelectron.* **2018**, *111*, 124−130.

(19) Zhou, M.; Wang, X.; Huang, K.; Huang, Y.; Hu, S.; Zeng, W. A fast, highly selective and sensitive dansyl-based fluorescent sensor for copper (II) ions and its imaging application in living cells. *Tetrahedron Lett.* **2017**, *58*, 991−994.

(20) Wei, M.; Zhang, Y.; Li, H.; Yao, S. A new "on−off" fluorescent probe for the selective detection of copper ions in living cells. *Anal. Methods* **2017**, *9*, 3956−3961.

(21) Quang, D. T.; Kim, J. S. Fluoro-and chromogenic chemo-dosimeters for heavy metal ion detection in solution and biospeci-mens. *Chem. Rev.* **2010**, *110*, 6280−6301.

(22) Yin, C.; Li, J.; Huo, F. Cu2+ biological imaging probes based on different sensing mechanisms. *Curr. Med. Chem.* **2019**, *26*, 3958−4002.

(23) Wang, Z.-G.; Ding, X.-J.; Huang, Y.-Y.; Yan, X.-J.; Ding, B.; Li, Q.-Z.; Xie, C.-Z.; Xu, J.-Y. The development of coumarin Schiff base system applied as highly selective fluorescent/colorimetric probes for Cu2+ and tumor biomarker glutathione detection. *Dyes Pigm.* **2020**, *175*, No. 108156.

(24) Zhang, Y.; Li, L.; Wang, J.; Jia, L.; Yang, R.; Guo, X. A 4, 5-quinolimide-based fluorescent sensor for sequential detection of Cu2+ and cysteine in water and living cells with application in a memorized device. *Spectrochim. Acta, Part A* **2020**, *230*, No. 118030.

(25) Baslak, C.; Kursunlu, A. N. A naked-eye fluorescent sensor for copper (II) ions based on a naphthalene conjugate Bodipy dye. *Photochem. Photobiol. Sci.* **2018**, *17*, 1091−1097.

(26) Jung, J.; Jo, J.; Dinescu, A. Rapid turn-on fluorescence detection of copper (II): Aromatic substituent effects on the response rate. *Org. Process Res. Dev.* **2017**, *21*, 1689−1693.

(27) Xu, Z.; Deng, P.; Li, J.; Tang, S. Fluorescent ion-imprinted sensor for selective and sensitive detection of copper (II) ions. *Sens. Actuators, B* **2018**, *255*, 2095−2104.

(28) Guan, M.; Xu, C.; Ma, J.; Yang, T.; Liu, J.; Feng, G. A Conjugated Polymer Fluorescent Sensor for Continuous Identification of Copper (II) and Pyrophosphate in Blood Serum and Synovial Fluid. *Anal. Sci.* **2019**, *35*, 625−630.

(29) Kim, H. J.; Quang, D. T.; Hong, J.; Kang, G.; Ham, S.; Kim, J. S. Ratiometry of monomer/excimer emissions of dipyrenyl calix [4] arene in aqueous media. *Tetrahedron* **2007**, *63*, 10788−10792.

(30) Fu, Y.; Pang, X.-X.; Wang, Z.-Q.; Chai, Q.; Ye, F. A highly sensitive and selective fluorescent probe for determination of Cu (II) and application in live cell imaging. *Spectrochim. Acta, Part A* **2019**, *208*, 198−205.

(31) Zhang, B.; Liu, H.; Wu, F.; Hao, G.; Chen, Y.; Tan, C.; Tan, Y.; Jiang, Y. A dual-response quinoline-based fluorescent sensor for the detection of Copper (II) and Iron (III) ions in aqueous medium. *Sens. Actuators, B* **2017**, *243*, 765−774.

(32) Kim, J. S.; Quang, D. T. Calixarene-derived fluorescent probes. *Chem. Rev.* **2007**, *107*, 3780−3799.

(33) Geissler, P. L. Temperature dependence of inhomogeneous broadening: On the meaning of isosbestic points. *J. Am. Chem. Soc.* **2005**, *127*, 14930−14935.

(34) Suzuki, T.; Yamamoto, R.; Higuchi, H.; Hirota, E.; Ohkita, M.; Tsuji, T. Electrochiroptical response of a hexaarylethane derivative with a helical π-skeleton: Drastic UV−Vis and CD spectral changes

upon electrolysis of 4′, 5′-dibromodispiro [xanthene-9, 9′(9′ H, 10′ H)-phenanthrene-10′, 9 ″-xanthene]. *J. Chem. Soc., Perkin Trans. 2* **2002**, 1937−1942.

(35) Kondo, S.-i.; Nagamine, M.; Karasawa, S.; Ishihara, M.; Unno, M.; Yano, Y. Anion recognition by 2, 2′-binaphthalene derivatives bearing urea and thiourea groups at 8-and 8′-positions by UV−vis and fluorescence spectroscopies. *Tetrahedron* **2011**, *67*, 943−950.

(36) More, K. N.; Lim, T.-H.; Kang, J.; Yun, H.; Yee, S.-T.; Chang, D.-J. Asymmetric and Reduced Xanthene Fluorophores: Synthesis, Photochemical Properties, and Application to Activatable Fluorescent Probes for Detection of Nitroreductase. *Molecules* **2019**, *24*, 3206.

(37) Mohammadi, A.; Ghasemi, Z. A simple pyrimidine based colorimetric and fluorescent chemosensor for sequential detection of copper (II) and cyanide ions and its application in real samples. *Spectrochim. Acta, Part A* **2020**, *228*, No. 117730.

(38) Kumar, A.; Chae, P. S.; Kumar, S. A dual-responsive anthrapyridone-triazole-based probe for selective detection of Ni2+ and Cu2+: A mimetic system for molecular logic gates based on color change. *Dyes Pigm.* **2020**, *174*, No. 108092.

(39) Xie, H.-F.; Yu, C.-J.; Huang, Y.-L.; Xu, H.; Zhang, Q.-L.; Sun, X.-H.; Feng, X.; Redshaw, C. A turn-off fluorescent probe for the detection of Cu 2+ based on a tetraphenylethylene-functionalized salicylaldehyde Schiff-base. *Mater. Chem. Front.* **2020**, *4*, 1500−1506.

(40) Dong, W.; Wang, R.; Gong, X.; Liang, W.; Fan, L.; Song, S.; Dong, C. A ratiometric and far-red fluorescence "off-on" sensor for sequential determination of copper (II) and L-histidine based on FRET system between N-acetyl-L-cysteine-capped AuNCs and N, S, P co-doped carbon dots. *Microchim. Acta* **2020**, *187*, No. 299.

(41) Hien, N. K.; Bao, N. C.; Nhung, N. T. A.; Trung, N. T.; Nam, P. C.; Duong, T.; Kim, J. S.; Quang, D. T. A highly sensitive fluorescent chemosensor for simultaneous determination of Ag (I), Hg (II), and Cu (II) ions: Design, synthesis, characterization and application. *Dyes Pigm.* **2015**, *116*, 89−96.

(42) Valeur, B. Principles of steady-state and time-resolved fluorometric techniques. *Mol. Fluorescence: Princ. Appl.* **2001**, 155−199.

(43) Mahar, J.; Shabir, G.; Channar, P. A.; Saeed, A.; Belfield, K. D.; Irfan, M.; Ul-Hamid, A. Donor-Pi-Acceptor Fluorene Conjugates, Based on Chalcone and Pyrimidine Derivatives: an Insight into Structure-Property Relationship, Photophysical and Electrochemical Properties. *J. Fluoresc.* **2020**, *30*, 419−426.

(44) Adamo, C.; Scuseria, G. E.; Barone, V. Accurate excitation energies from time-dependent density functional theory: Assessing the PBE0 model. *J. Chem. Phys.* **1999**, *111*, 2889−2899.

(45) Ali, A.; Rafiq, M. I.; Zhang, Z.; Cao, J.; Geng, R.; Zhou, B.; Tang, W. TD-DFT benchmark for UV−visible spectra of fused-ring electron acceptors using global and range-separated hybrids. *Phys. Chem. Chem. Phys.* **2020**, *22*, 7864−7874.

(46) Coskun, D.; Jerome, S. V.; Friesner, R. A. Evaluation of the performance of the B3LYP, PBE0, and M06 DFT functionals, and DBLOC-corrected versions, in the calculation of redox potentials and spin splittings for transition metal containing systems. *J. Chem. Theory Comput.* **2016**, *12*, 1121−1128.

(47) Radhakrishnan, R.; Sreejalekshmi, K. Computational Design, Synthesis, and Structure Property Evaluation of 1, 3-Thiazole-Based Color-Tunable Multi-heterocyclic Small Organic Fluorophores as Multifunctional Molecular Materials. *J. Org. Chem.* **2018**, *83*, 3453−3466.

(48) Frisch, M. J.; Trucks, G. W.; Schlegel, H. B.; Scuseria, G. E.; Robb, M. A.; Cheeseman, J. R.; Scalmani, G.; Barone, V.; Mennucci, B.; Petersson, G. A.; Nakatsuji, H.; Caricato, M.; Li, X.; Hratchian, H. P.; Izmaylov, A. F.; J. Bloino, G. Z.; Sonnenberg, J. L.; Hada, M.; Ehara, M.; Toyota, K.; Fukuda, R.; Hasegawa, J.; Ishida, M.; Nakajima, T.; Honda, Y.; Kitao, O.; Nakai, H.; Vreven, T.; Montgomery, J. A., Jr.; P, J. E.; Ogliaro, F.; Bearpark, M.; Heyd, J. J.; Brothers, E.; Kudin, K. N.; Staroverov, V. N.; Keith, T.; Kobayashi, R.; Normand, J.; Raghavachari, K.; Rendell, A.; Burant, J. C.; Iyengar, S. S.; Tomasi, J.; Cossi, M.; Rega, N.; Millam, J. M.; Klene, M.; Knox, J. E.; Cross, J. B.; Bakken, V.; Adamo, C.; Jaramillo, J.; Gomperts, R.; Stratmann, R. E.; Yazyev, O.; Austin, A. J.; Cammi, R.; Pomelli, C.; Ochterski, J. W.; Martin, R. L.; Morokuma, K.; Zakrzewski, V. G.; Voth, G. A.; Salvador, P.; Dannenberg, J. J.; Dapprich, S.; Daniels, A. D.; Farkas, O.; Foresman, J. B.; Ortiz, J. V.; Cioslowski, J.; Fox, D. J. *Gaussian 09*, Revision A.02; Gaussian, Inc.: Wallingford CT, 2009.

(49) Bader, R. F. A quantum theory of molecular structure and its applications. *Chem. Rev.* **1991**, *91*, 893−928.

(50) Wojtulewski, S.; Grabowski, S. J. DFT and AIM studies on two-ring resonance assisted hydrogen bonds. *J. Mol. Struct: THEOCHEM* **2003**, *621*, 285−291.

(51) Koch, U.; Popelier, P. L. Characterization of CHO hydrogen bonds on the basis of the charge density. *J. Phys. Chem. A* **1995**, *99*, 9747−9754.

(52) Bader, R. F. W. *Atoms in Molecules: A Quantum Theory*; Oxford University Press: New York, 1990.

(53) Nhan, D. T.; Hien, N. K.; Van Duc, H.; Nhung, N. T. A.; Trung, N. T.; Van, D. U.; Shin, W. S.; Kim, J. S.; Quang, D. T. A hemicyanine complex for the detection of thiol biomolecules by fluorescence. *Dyes Pigm.* **2016**, *131*, 301−306.

(54) André, J.-M. *Exploring Aspects of Computational Chemistry: Concepts and Exercises 2 Volumes*; Presses universitaires de Namur, 1997.

(55) Reed, A. E.; Weinhold, F. Natural localized molecular orbitals. *J. Chem. Phys.* **1985**, *83*, 1736−1740.

(56) Reed, A. E.; Weinstock, R. B.; Weinhold, F. Natural population analysis. *J. Chem. Phys.* **1985**, *83*, 735−746.

(57) Osman, O. I. DFT study of the structure, reactivity, natural bond orbital and hyperpolarizability of thiazole azo dyes. *Int. J. Mol. Sci.* **2017**, *18*, 239.